Emergent Periodic and Quasiperiodic Lattices on Surfaces of Synthetic Hall Tori and Synthetic Hall Cylinders

Yangqian Yan[1], Shao-Liang Zhang,[2] Sayan Choudhury,[1] and Qi Zhou[1]

[1]*Department of Physics and Astronomy, Purdue University, West Lafayette, Indiana 47907, USA*
[2]*School of Physics, Huazhong University of Science and Technology, Wuhan 430074, People's Republic of China*

Synthetic spaces allow physicists to bypass constraints imposed by certain physical laws in experiments. Here, we show that a synthetic torus, which consists of a ring trap in the real space and internal states of ultracold atoms cyclically coupled by Laguerre-Gaussian Raman beams, could be threaded by a net effective magnetic flux through its surface—an impossible mission in the real space. Such a synthetic Hall torus gives rise to a periodic lattice in real dimensions, in which the periodicity of the density modulation of atoms fractionalizes that of the Hamiltonian. Correspondingly, the energy spectrum is featured by multiple bands grouping into clusters with nonsymmorphic-symmetry-protected band crossings in each cluster, leading to swaps of wave packets in Bloch oscillations. Our scheme allows physicists to glue two synthetic Hall tori such that localization may emerge in a quasicrystalline lattice. If the Laguerre-Gaussian Raman beams and ring traps were replaced by linear Raman beams and ordinary traps, a synthetic Hall cylinder could be realized and deliver many of the aforementioned phenomena.

Spaces with nontrivial topologies provide quantum systems unprecedented properties [1–7]. As a prototypical space of a finite genus, the importance of a torus in modern physics is more far reaching than applying periodic boundary conditions (PBC) in theoretical calculations. It plays a crucial role in quantum Hall physics. The ground state of a fractional quantum Hall state becomes degenerate on a torus or any surface with a finite genus [8]. Such degeneracy, which is unavailable on a cylinder or a flat space and defines the concept of the topological order lays the foundation of topological quantum computation [9]. However, due to the absence of magnetic monopoles in nature, it is impossible to generate a net magnetic flux through a closed surface in the real space. The study of quantum Hall states on a torus has eluded experiments so far.

Ultracold atoms provide physicists a unique platform to engineer Hamiltonians and allow physicists to achieve many quantum Hall states unattainable in electronic systems [10], such as quantum Hall states of bosons and quantum Hall states with high spins. Other than the typical harmonic potentials, ring traps have been implemented in an annular geometry [11,12]. Linear and Laguerre-Gaussian (LG) Raman beams have been used to create spin-momentum coupling and spin-angular momentum coupling, respectively [13–17]. If one considers the internal degree of freedom as a synthetic dimension, the spin-momentum coupling gives rise to a synthetic magnetic field in a two-dimensional plane [18,19]. Whereas experiments have been focusing on open boundary conditions in the synthetic dimension [20,21], there have been theoretical

proposals on creating a periodic or twisted boundary condition [22–27]. However, few experiments has fulfilled the requirements of these proposals [28,29].

We propose a simple scheme to realize a synthetic torus penetrated by a net effective magnetic flux. Ultracold atoms confined in a ring trap in the real space are subjected to spin-angular momentum coupling induced by LG Raman beams. Either hyperfine spins or nuclear spins could be used to enable a cyclic coupling and form a loop in the discrete synthetic dimension. Cyclic couplings have been studied for different purposes, including realizing two-dimensional spin-orbit coupling and creating Yang monopoles [30–32]. Here, we use spin-angular momentum coupling to synthesize internal states and real dimensions into a synthetic Hall torus. PBCs in both synthetic and real dimensions deliver a torus. Spin-angular momentum coupling produces finite effective magnetic fluxes penetrating its toroidal surface, signifying the rise of a synthetic Hall torus. Replacing Laguerre-Gaussian Raman beams by linear ones, our scheme applies to ordinary traps with open boundary conditions for creating synthetic Hall cylinders, which have been realized by experiments recently [28,29].

We further unfold unique properties of synthetic Hall tori and cylinders. Unlike previous works including optical lattices in the real dimension [20,21,24,26–28], we consider a continuous real space trap. Interestingly, periodic or quasiperiodic lattices emerge in the continuous real dimension, as a result of PBC in the synthetic dimension. The periodic lattice modulates the density of atoms with a fractionalized periodicity of the Hamiltonian and a unique band structure shows up. Energy bands form clusters with
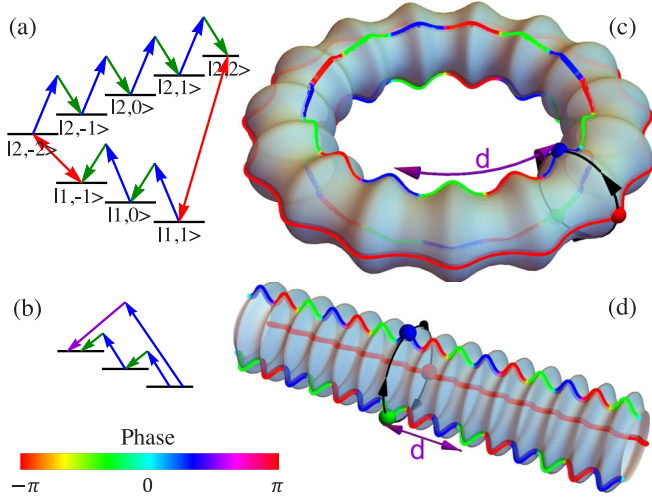
FIG. 1.   (a) Energy diagram for the hyperfine states and the laser coupling scheme. Blue and green arrows represent the Raman coupling. Bidirectional arrows represent microwave couplings. (b) Simplified coupling diagram for three internal states coupled by Raman beams. (c)–(d) Torus (cylinder) formed by three cyclically coupled internal states in a real space ring trap. The density oscillation is depicted as the fluctuation of the radius of the torus or cylinder. Colored curves represent phases of the wave function of each spin component.

nonsymmorphic-symmetry-protected band crossings in each cluster. Wave packets in each cluster swap with each other in Bloch oscillations. Though each single synthetic Hall torus or cylinder supports only extend states, once two of them are glued together, quasiperiodic lattices may emerge and lead to localized states in the real space. Such "localization from gluing" demonstrates the power of synthetic Hall tori or cylinders in accessing even more complex synthetic spaces and intriguing quantum phenomena there.

Proposed scheme and Hamiltonian.—We consider M internal states in a real space ring trap. For alkali atoms, these M spins involves both $F = 1$ and $F = 2$, as shown in Fig. 1(a). At weak magnetic fields, linear Zeeman splitting dominates; thus a single pair of LG Raman beams simultaneously couples every consecutive state within each manifold; microwave fields couple $|1,1\rangle$ ($|1,-1\rangle$) and $|2,2\rangle$ ($|2,-2\rangle$). These eight states form a circle in the synthetic dimension. Because of the opposite g factors between $F = 1$ and $F = 2$, a finite angular momentum transfer occurs once an atom finishes the loop in the synthetic dimension. A net effective magnetic flux emerges on the torus. Each hyperfine spin state has multiple angular momenta.

The number of internal states are controllable. On the one hand, at large magnetic fields, quadratic Zeeman splittings become important, and fewer spins can be separated out from the rest to form a smaller circle [26,28–30,32]. Note that shrinking the synthetic dimension does not change any results qualitatively, as fractional quantum Hall states can

be adiabatically connected to 1D charge-density waves [33]. Chiral edge currents in the quantum Hall strips have also been observed using only three internal states [20,21]. On the other hand, using the $^1S_0$ and $^3P_0$ states of Sr87 [34], one could cyclically couple up to 20 internal states.

Here, we consider nearest neighbors in the synthetic dimension coupled by LG Raman beams. The spin flip from the jth spin state to the $j + 1$th one is thus accompanied by an angular momentum increase $m_{j,j+1}$, which is the difference between the angular momenta carried by the two LG beams. A microwave coupling then corresponds to $m_{j,j+1} = 0$.

We define the position $x = \phi L/(2\pi)$ and the momentum $p = 2\pi m/L$, where ϕ is the azimuthal angle and L is the circumference of the real space ring. We also define $q_{j,j+1} = 2\pi m_{j,j+1}/L$ as the "momentum" transfer along the azimuthal direction. The advantage of the notation is that all results directly apply to a cylinder. In both the cylinder and the torus, x represents the direction in the real dimension. The Hamiltonian reads

$$
H = \sum_{j=1}^{M} |\psi^j(x)\rangle \left(-\frac{\hbar^2}{2m_0} \partial_x^2 + \epsilon_j \right) \langle \psi^j(x)|
$$
$$
+ \sum_{j=1}^{M} (\Omega_{j,j+1} e^{iq_{j,j+1}x} |\psi^{j+1}(x)\rangle \langle \psi^j(x)| + \text{H.c.}), \quad (1)
$$

where $\psi^j(x)$ denotes the spatial wave function for the jth spin, ϵ_j the one (two) photon detuning in the microwave (Raman) transition, $\Omega_{j,j+1}$ the coupling strength between the jth and the $j + 1$th spin state, and $\psi^{M+1}(x) = \psi^1(x)$. Whereas our results are very general and do not require tuning every single parameter arbitrarily, quadratic Zeeman splitting could create uneven energy separations and each pair of hyperfine spin states could be coupled by different lasers. Thus, $\Omega_{j,j+1}$ can be, in principle, tuned independently. The total phase accumulated after an atom finishes a circle $j \to j + 1 \to j + 2 \ldots \to j - 1 \to j$, $\varphi(x) \equiv e^{iQx}$ is finite and spatially dependent, where $Q \equiv \sum_{j=1}^{M} q_{j,j+1}$. The total synthetic magnetic flux on the surface of the torus per unit length in the physical dimension is then proportional to Q.

Nonsymmorphic symmetry and band structures.— We start from commensurate momentum transfers, i.e., $q_{j,j+1} = n_j q_L$, where n_j are integers. For any coupling strengths $\Omega_{j,j+1}$, the reciprocal lattice vector q_L determines the periodicity of $H(x)$, $H(x) = H[x + (2\pi/q_L)]$. If one of these couplings vanishes, the phases $e^{iq_{j,j+1}}$ can be absorbed to $|\psi^{j+1}(x)\rangle$, and any spin component in an eigenstate contains a single plane wave. In contrast, when all $\Omega_{j,j+1} \neq 0$, the phases cannot be gauged away under such PBC. A single spin component in any eigenstate contains multiple plane waves and the densities form standing

waves. The lattice in the real space is therefore an emergent one from the PBC in the synthetic dimension.

The Bloch wave functions $\vec{\psi}_k(x)$ are simultaneous eigenstates of H and $\hat{T}(d)$ $[\hat{T}(d)\vec{\psi}_k(x) = e^{ikd}\vec{\psi}_k(x)]$, where $\vec{\psi}(x)$ is an M-component wave function, k the quasimomentum, $d \equiv 2\pi/q_L$ the lattice spacing, and $T(d)$ the translation operator of distance d. We define the non-symmorphic symmetry operator $\hat{G}$ as a combination of a translation for a fraction of the lattice space $T(2\pi/Q)$ in the real dimension and a unitary transformation U_s in the synthetic direction,

$$x \rightarrow x + \frac{2\pi}{Q}, \qquad |\psi^{j>1}\rangle \rightarrow e^{-i(2\pi/Q)\sum_{j'=1}^{j-1} q_{j',j'+1}}|\psi^j\rangle. \quad (2)$$

Again, it is understood that $M+1$ is equivalent to 1. A simple example of the nonsymmorphic symmetry is the glide-reflection symmetry, a translation for half of the lattice spacing combined with a reflection in the perpendicular direction, which has played an important role in topological quantum matters [35–37]. Consider a special case $\epsilon_j = 0$, $\Omega_{j,j+1} = \bar{\Omega}$, and $n_j = \bar{n}$; the synthetic dimension becomes translational invariant in the real dimension. $\hat{G}$ and its multiples, together with the translation in the synthetic dimension, then form the conventional magnetic translation group [38]. In generic cases where the synthetic dimension does not have translation invariance, i.e., nonuniform ϵ_j, $\Omega_{j,j+1}$, or n_j. $[H, \hat{G}] = 0$ is still satisfied and signifies a nonsymmorphic symmetry.

We define $n \equiv Q/q_L = \sum_{j=1}^{M} n_j$. Many physical quantities depend on n; i.e., the properties of the system crucially rely on how the synthetic magnetic field is distributed on the surface of the torus, not just the total flux. Applying $\hat{G}$ for n times is equivalent to a translation in the physical dimension for one lattice spacing, $\hat{G}^n \vec{\psi}_k(x) = e^{ikd}\vec{\psi}_k(x)$. Thus,

$$\hat{G}\vec{\psi}_k(x) = c_s\vec{\psi}_k(x), \qquad c_s = e^{i[(kd/n)+(2s\pi/n)]}, \quad (3)$$

where $s = 1, 2, \ldots, n-1, n$. Equation (3) shows that, as the quasimomentum k changes by a reciprocal lattice vector q_L, the eigenvalue of $\hat{G}$ changes by $e^{2i\pi/n}$; i.e., the sth eigenvalue becomes the $s+1$ one. Meanwhile, $\vec{\psi}_k(x) = \vec{\psi}_{k+q}(x)$ is satisfied. Thus, we conclude that bands must form clusters, each of which contains n bands. These n bands are the n eigenstates of the operator $\hat{G}$ with the sth eigenvalue c_s, and intersect with each other within the Brillouin zone (BZ).

We solve H in Eq. (1) using plane-wave expansions. The band structure fully agrees with the prediction from the above symmetry considerations. Figure 2(a) shows the energy bands when $M = 3$, $q_{1,2} = q_{2,3} = q_{3,1} = q$, and coupling strength $\Omega_{1,2} = 1.2E_R$, $\Omega_{2,3} = 1.8E_R$, and $\Omega_{3,1} = 1.5E_R$, where $E_R = \hbar^2 Q^2/2m_0$ is the recoil energy defined
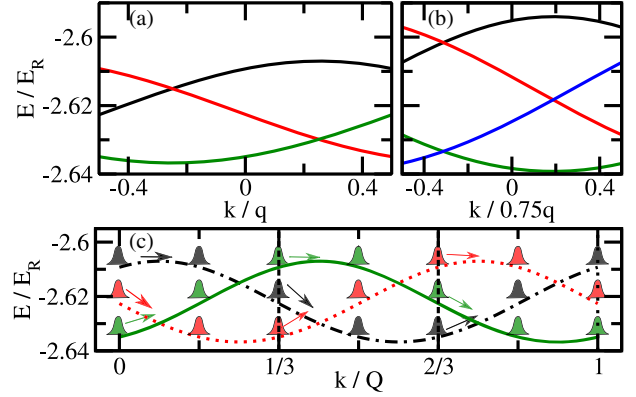

FIG. 2. Band structures when $q_{1,2}: q_{2,3}: q_{3,1} = 1: 1: 1$(a) and $q_{1,2}: q_{2,3}: q_{3,1} = 1: 1: 2$ (b). (c) Bloch oscillation for (a). Vertical lines represent the boundaries of the BZ.

by Q. Here, the reciprocal lattice vector $q_L = q$ and $n = Q/q_L = 3$. The cylindrical or toroidal surface is penetrated by a uniform flux. Thus, three bands exist in each cluster. The eigenstate of the sth band is

$$\vec{\psi}_k(x) = e^{i(k+sq)x}(u_k^1(x), u_k^2(x), u_k^3(x))^T,$$

$$u_k^j(x) = e^{i(j-1)qx} \sum_{l=-\infty}^{\infty} c_l^j(k)e^{ilQx}, \quad (4)$$

where $u_k^j(x)$ is the periodic Bloch wave function of the jth spin state, l an integer, and $c_l^j(k)$ determined by Eq. (1). The density of the jth spin state, $\rho_k^j(x) \equiv |u_k^j(x)|^2$ satisfies

$$\rho_k^j(x) = \rho_k^j\left(x + \frac{2\pi}{Q}\right) = \rho_k^j\left(x + \frac{d}{3}\right). \quad (5)$$

The total density $\rho(x) = \sum_j \rho_k^j(x)$, by definition, also satisfies Eq. (5) [39]. Despite the continuous real dimension, the density of atoms oscillates with a period only $1/3$ of that of the Hamiltonian, as shown in Figs. 1(c)–1(d). In contrast, the relative phase between $u_k^2(x)$ $[u_k^3(x)]$ and $u_k^1(x)$ has a periodicity of d, as shown by the colored curves in Figs. 1(c)–1(d). As previously discussed, such results crucially depend on the PBC. Both periodic density and phase oscillations vanish once the synthetic dimension has an open boundary condition.

Swapping wave packets in Bloch oscillations.—When a constant force is applied, a wave packet in the momentum space experiences a Bloch oscillation, which has exactly the same period of the Hamiltonian in an ordinary band structure. In contrast, the period of the Bloch oscillation here is given by $3q$, tripling the reciprocal lattice vector. Because of the presence of band crossings, a wave packet does not return to the original band after the momentum changes by q. Instead, it swaps with another wave packet from a different band.

The significance of such Bloch oscillations here is that it traces the Wilson lines, a path-ordered integral of

non-Abeliean Berry connections in the momentum space [40,41]. Because of the nonsymmorphic-symmetry-protected band crossings, Abelian Berry connections no longer apply when studying topological properties of the band structure. Non-Abelian Berry connections and the Wilson lines characterize how a quantum state changes to a different one while the Hamiltonian returns to the original one [42,43], a prototypical non-Abelian operation. This is precisely what we see from Fig. 2(c). If we label the bands as 1,2,3 from bottom to top based on the energies, the green wave packet initially at band-1 moves to band-3, meanwhile the red (black) one initially at band-2 (band-3) moves to band-1 (band-2) when $\Delta k = q$ [44]. When $\Delta k = Q = 3q$, these three wave packets swap with each other for six times, as shown in Fig. 2(c).

The above discussions can be directly generalized to other choices of $\{q_{j,j+1}\}$. If $q_{1,2} = q_{2,3} = \frac{3}{4}q$, $q_{3,1} = \frac{3}{2}q$, though the total momentum transferred, Q, is still $3q$, the same as the previously discussed case, q_L becomes $3q/4$ and $n = 4$. One third of the surface has a larger magnetic flux than the remaining region [44], and a cluster consists of four bands [Fig. 2(b)]. Changing the value of some of the wave vectors is equivalent to redistributing the magnetic flux on the surface, and leads to distinct band structures. We emphasize that the total number of states of the system remains unchanged. The change of the number of bands is associated with the change of the BZ. In this example, the reciprocal lattice vector q'_L become $\frac{3}{4}q$. Shrinking the size of the BZ then leads to an increase in the number of bands in a cluster.

Quasiperiodic lattices.—If $q_{j,j+1}$ are incommensurate, e.g., $q_{1,2}:q_{2,3}:\cdots:q_{M,1} = 1:1:\cdots:\gamma$, where $\gamma = [(\sqrt{5}-1)/2]$, a peculiar quasiperiodic lattice arises: certain quantities have well-defined periodicities but others do not. For example, Eqs. (4) hold for a generic $\{q_{j,j+1}\}$ when $M = 3$. Though H in Eq. (1) is aperiodic, the density of each spin still satisfies $\rho^j_k(x) = \rho^j_k[x + (2\pi/Q)]$. The wave function of each spin component is still extended, as its plane wave expansion only includes multiples of Q. In contrast, the relative phases between different spin components are spatially variant and are not commensurate. Thus, the wave function $\psi_k(x)$ is aperiodic in the real dimension. Defining a pseudospin-1, $S_\mu = \sum_{j,j'} u^{j*}_k(x)\mathcal{F}^{j,j'}_\mu u^{j'}_k(x)$, where $j, j' = 1, 2, 3$, $\mathcal{F}^{j,j'}_\mu$ are the spin-1 Pauli matrices, and $\mu = x, y, z$. $S_z(x)$ is periodic, $S_z(x) = S_z(x + 2\pi/Q)$, but $S_x(x)$ and $S_y(x)$ do not have well defined periods, as shown in Fig. 3(a).

On a cylinder, there is no restriction on the choice of $q_{j,j+1}$. In contrast, an irrational ratio $q_{j,j+1}/q_{j',j'+1}$ is not allowed on a torus, as the PBC in the real dimension require that all momentum scales are multiples of $2\pi/L$. Nevertheless, any irrational number can be approached by the ratio of two integers with increasing the integers' values. For instance, γ can be approximated by
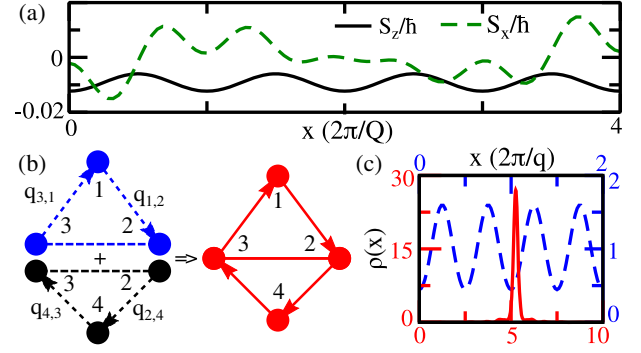

FIG. 3. (a) Spin polarization along the x and z directions as a function of x. (b) Schematic of the cross sections of two tori or cylinders when they are glued together. (c) Total density of the ground eigenstate at zero quasimomentum before (dashed line, only the top blue torus or cylinder is shown) and after (solid line) the gluing. $q_{1,2} = q_{3,1} = q$, $q_{2,3} = 0$, $q_{2,4} = q_{4,3} = \gamma q$, and all couplings $\Omega_{j,j'}$ are $2E_r$, where $E_r = \hbar^2 q^2/2m_0$ is the recoil energy defined by q. $\gamma_8 = 13/21$ has been used as an approximation of $\gamma = (\sqrt{5}-1)/2$.

$\gamma_\alpha = a_{\alpha-1}/a_\alpha$, where $\{a_\alpha\}$ is the Fibonacci series $1, 1, 2, 3, 5\ldots$, with increased accuracy. When the approximation order α increases, the periodicity of $S_{x,y}(x)$ increases. γ_α with a small α well reproduces the result for a small x and a large γ.

Localization by gluing.—Our scheme can be implemented to access more complex synthetic spaces. For instance, adding extra couplings to the synthetic dimension is equivalent to gluing multiple tori or cylinders. Figure 3(b) shows that two tori or cylinders with $M = 3$ can be glued to a single one with $M = 4$. In the real space, it is difficult to realize such gluing, as it is required to identify certain parts of two different objects. Using the synthetic dimension, adding an additional tunneling through the interior of single tori or cylinder with $M = 4$, $\Omega' = \Omega_{2,3}$, immediately realizes this gluing and delivers a system with a different topology. Though each single torus or cylinder supports only extended eigenstates, after gluing them together, eigenstates at low energies could become localized, as shown in Fig. 3(c) [45]. The wave function of a single spin component now includes multiple momentum scales, $q_{1,2}$, and $q_{4,3}$, unlike a single torus or cylinder case where only Q is relevant. The interference of plane waves with incommensurate wave vectors could thus potentially localize the wave function.

To quantitatively characterize the localization, we compute the width of the lowest band as a function of Ω'. It has been shown that the ground bandwidth scales with a_α^{-2} for extended states, and decays much faster for localized states [46,47]. Here, the scaled bandwidth almost vanishes at an intermediate value of Ω', where eigenstates are localized, as shown in Fig. 4. When Ω' is very small, the wave function is still extended, similar to a single torus without Ω'. For large Ω', dominating contributions to the wave function
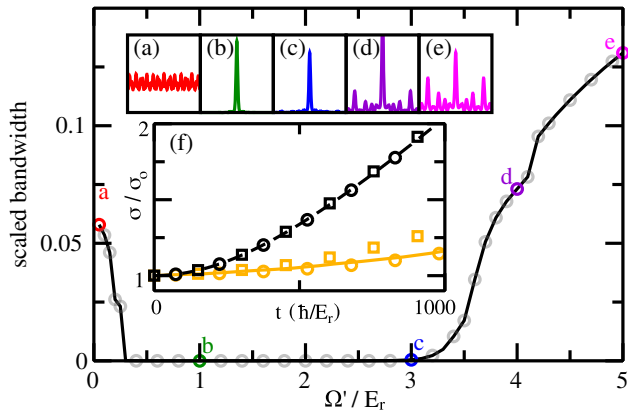
FIG. 4. Bandwidth multiplied by a_α^2/E_r as a function of Ω' for $\alpha = 12$. The insets (a), ..., (e) show the corresponding zero quasimomentum ground state at $\Omega'/E_r = 0.05, 1, 3, 4, 5$, respectively, with $\alpha = 8$. (f) The width of the Gaussian wave packet as a function of time The solid orange (black dashed) curve represents noninteracting results for $\Omega' = 2E_r$ ($\Omega' = 0$). Squares and circles represent results for $\int g\rho_i^2 dx = \pm 0.003 E_r$, respectively, where ρ_i is the density for the initial state.

come from only two hyperfine spin states [2 and 3 in Fig. 3(b)] such that the incommensurate wave vectors are no longer relevant and the wave function is still extended.

The localization can also be characterized by the expansion of an initially localized wave packet with a width σ_0 in real space. We consider a Gaussian wave packet as the initial state. For small or large Ω', where the eigenstates at low energies are delocalized, the width of the wave packet σ increases quickly. In contrast, σ grows much slower in the localized regime. To further consider interaction effects, we numerically solve a time-dependent Gross-Pitaevskii equation,

$$i\hbar \frac{\partial \vec{\psi}(x)}{\partial t} = (\hat{H} + g\rho)\vec{\psi}(x), \qquad (6)$$

where g is the interaction strength. We find that a weak repulsive (attractive) interaction slightly enhances (suppresses) the dynamics. In addition, we have considered the ground state of interacting bosons in the trap. The main conclusions remain unchanged [44].

We have shown that atom-laser interactions allow physicists to synthesize Hall tori and cylinders hosting intriguing quantum phenomena in the emergent periodic and quasiperiodic lattices. We hope that our results will stimulate more works on synthetic spaces so as to explore physics that are not easy to access in conventional traps.

[1] H. Kleinert, *Gauge Fields in Condensed Matter* (World Scientific, Singapore, 1989).

[2] C. Schulte, Quantum Mechanics on the Torus, Klein Bottle and Projective Sphere, in *Symmetries Sci. IX* (Springer US, Boston, MA, 1997), pp. 313–323.

[3] K. Kaneda and Y. Okabe, Finite-Size Scaling for the Ising Model on the Möbius Strip and the Klein Bottle, Phys. Rev. Lett. **86**, 2134 (2001).

[4] W. T. Lu and F. Y. Wu, Ising model on nonorientable surfaces: Exact solution for the Möbius strip and the Klein bottle, Phys. Rev. E **63**, 026107 (2001).

[5] A. M. Turner, V. Vitelli, and D. R. Nelson, Vortices on curved surfaces, Rev. Mod. Phys. **82**, 1301 (2010).

[6] T.-L. Ho and B. Huang, Spinor Condensates on a Cylindrical Surface in Synthetic Gauge Fields, Phys. Rev. Lett. **115**, 155304 (2015).

[7] N.-E. Guenther, P. Massignan, and A. L. Fetter, Quantized superfluid vortex dynamics on cylindrical surfaces and planar annuli, Phys. Rev. A **96**, 063608 (2017).

[8] X. G. Wen and Q. Niu, Ground-state degeneracy of the fractional quantum Hall states in the presence of a random potential and on high-genus Riemann surfaces, Phys. Rev. B **41**, 9377 (1990).

[9] A. Y. Kitaev, Fault-tolerant quantum computation by anyons, Ann. Phys. (N. Y.) **303**, 2 (2003).

[10] I. Bloch, J. Dalibard, and W. Zwerger, Many-body physics with ultracold gases, Rev. Mod. Phys. **80**, 885 (2008).

[11] O. Morizot, Y. Colombe, V. Lorent, H. Perrin, and B. M. Garraway, Ring trap for ultracold atoms, Phys. Rev. A **74**, 023617 (2006).

[12] S. Eckel, J. G. Lee, F. Jendrzejewski, N. Murray, C. W. Clark, C. J. Lobb, W. D. Phillips, M. Edwards, and G. K. Campbell, Hysteresis in a quantized superfluid 'atomtronic' circuit, Nature (London) **506**, 200 (2014).

[13] Y. J. Lin, K. Jiménez-García, and I. B. Spielman, Spin-orbit-coupled Bose-Einstein condensates, Nature (London) **471**, 83 (2011).

[14] K. Sun, C. Qu, and C. Zhang, Spin–orbital-angular-momentum coupling in Bose-Einstein condensates, Phys. Rev. A **91**, 063627 (2015).

[15] L. Chen, H. Pu, and Y. Zhang, Spin-orbit angular momentum coupling in a spin-1 Bose-Einstein condensate, Phys. Rev. A **93**, 013629 (2016).

[16] H.-R. Chen, K.-Y. Lin, P.-K. Chen, N.-C. Chiu, J.-B. Wang, C.-A. Chen, P.-P. Huang, S.-K. Yip, Y. Kawaguchi, and Y.-J. Lin, Spin–Orbital-Angular-Momentum Coupled Bose-Einstein Condensates, Phys. Rev. Lett. **121**, 113204 (2018).

[17] D. Zhang, T. Gao, P. Zou, L. Kong, R. Li, X. Shen, X.-L. Chen, S.-G. Peng, M. Zhan, H. Pu, and K. Jiang, Ground-State Phase Diagram of a Spin-Orbital-Angular-Momentum Coupled Bose-Einstein Condensate, Phys. Rev. Lett. **122**, 110402 (2019).

[18] A. Celi, P. Massignan, J. Ruseckas, N. Goldman, I. B. Spielman, G. Juzeliūnas, and M. Lewenstein, Synthetic Gauge Fields in Synthetic Dimensions, Phys. Rev. Lett. **112**, 043001 (2014).

[19] E. Anisimovas, M. Račiūnas, C. Sträter, A. Eckardt, I. B. Spielman, and G. Juzeliūnas, Semisynthetic zigzag optical lattice for ultracold bosons, Phys. Rev. A **94**, 063632 (2016).

[20] B. K. Stuhl, H. I. Lu, L. M. Aycock, D. Genkina, and I. B. Spielman, Visualizing edge states with an atomic Bose gas in the quantum Hall regime, Science **349**, 1514 (2015).

[21] M. Mancini, G. Pagano, G. Cappellini, L. Livi, M. Rider, J. Catani, C. Sias, P. Zoller, M. Inguscio, M. Dalmonte, and L. Fallani, Observation of chiral edge states with neutral fermions in synthetic Hall ribbons, Science **349**, 1510 (2015).

[22] F. Grusdt and M. Höning, Realization of fractional Chern insulators in the thin-torus limit with ultracold bosons, Phys. Rev. A **90**, 053623 (2014).

[23] O. Boada, A. Celi, J. Rodríguez-Laguna, J. I. Latorre, and M. Lewenstein, Quantum simulation of non-trivial topology, New J. Phys. **17**, 045007 (2015).

[24] M. Łącki, H. Pichler, A. Sterdyniak, A. Lyras, V. E. Lembessis, O. Al-Dossary, J. C. Budich, and P. Zoller, Quantum Hall physics with cold atoms in cylindrical optical lattices, Phys. Rev. A **93**, 013604 (2016).

[25] J. C. Budich, A. Elben, M. Łącki, A. Sterdyniak, M. A. Baranov, and P. Zoller, Coupled atomic wires in a synthetic magnetic field, Phys. Rev. A **95**, 043632 (2017).

[26] L. Taddia, E. Cornfeld, D. Rossini, L. Mazza, E. Sela, and R. Fazio, Topological Fractional Pumping with Alkaline-Earth-Like Atoms in Synthetic Lattices, Phys. Rev. Lett. **118**, 230402 (2017).

[27] H. Kim, G. Zhu, J. V. Porto, and M. Hafezi, Optical Lattice with Torus Topology, Phys. Rev. Lett. **121**, 133002 (2018).

[28] J. H. Han, J. H. Kang, and Y.-i. Shin, Band Gap Closing in a Synthetic Hall Tube of Neutral Fermions, Phys. Rev. Lett. **122**, 065303 (2019).

[29] C.-H. Li, Y. Yan, S. Choudhury, D. B. Blasing, Q. Zhou, and Y. P. Chen, A Bose-Einstein condensate on a synthetic Hall cylinder, arXiv:1809.02122.

[30] D. L. Campbell, G. Juzeliūnas, and I. B. Spielman, Realistic Rashba and Dresselhaus spin-orbit coupling for neutral atoms, Phys. Rev. A **84**, 025602 (2011).

[31] L. Huang, Z. Meng, P. Wang, P. Peng, S.-L. Zhang, L. Chen, D. Li, Q. Zhou, and J. Zhang, Experimental realization of two-dimensional synthetic spin–orbit coupling in ultracold Fermi gases, Nat. Phys. **12**, 540 (2016).

[32] S. Sugawa, F. Salces-Carcoba, A. R. Perry, Y. Yue, and I. B. Spielman, Second Chern number of a quantum-simulated non-Abelian Yang monopole, Science **360**, 1429 (2018).

[33] A. Seidel and D.-H. Lee, Abelian and Non-Abelian Hall Liquids and Charge-Density Wave: Quantum Number Fractionalization in One and Two Dimensions, Phys. Rev. Lett. **97**, 056804 (2006).

[34] M. M. Boyd, T. Zelevinsky, A. D. Ludlow, S. M. Foreman, S. Blatt, T. Ido, and J. Ye, Optical atomic coherence at the 1-second time scale, Science **314**, 1430 (2006).

[35] K. Shiozaki, M. Sato, and K. Gomi, Z_2 topology in nonsymmorphic crystalline insulators: Möbius twist in surface states, Phys. Rev. B **91**, 155120 (2015).

[36] C. Fang and L. Fu, New classes of three-dimensional topological crystalline insulators: Nonsymmorphic and magnetic, Phys. Rev. B **91**, 161105(R) (2015).

[37] Q.-Z. Wang and C.-X. Liu, Topological nonsymmorphic crystalline superconductors, Phys. Rev. B **93**, 020505(R) (2016).

[38] J. Zak, Magnetic translation group, Phys. Rev. **134**, A1602 (1964).

[39] We normalize the wave function according to $\int_0^{2\pi} |\vec{\psi}(\phi)|^2 d\psi = 2\pi$ ($\int_0^L |\vec{\psi}(\phi)|^2 dx = L$) for the torus (cylinder), where L should be multiples of the period of the underlying Hamiltonian. Thus, the wave function and the density is dimensionless in both cases.

[40] T. Li, L. Duca, M. Reitter, F. Grusdt, E. Demler, M. Endres, M. Schleier-Smith, I. Bloch, and U. Schneider, Bloch state tomography using Wilson lines, Science **352**, 1094 (2016).

[41] S.-L. Zhang and Q. Zhou, Two-leg Su-Schrieffer-Heeger chain with glide reflection symmetry, Phys. Rev. A **95**, 061601(R) (2017).

[42] F. Wilczek and A. Zee, Appearance of Gauge Structure in Simple Dynamical Systems, Phys. Rev. Lett. **52**, 2111 (1984).

[43] M. Fruchart, Y. Zhou, and V. Vitelli, Dualities and non-Abelian mechanics, arXiv:1904.07436.

[44] See Supplemental Material at http://link.aps.org/supplemental/10.1103/PhysRevLett.123.260405 for Bloch oscillation in the presence the band crossings, interaction effects on the expansion of the Gaussian wave packet in real space, expansion dynamics of the ground state in the harmonic trap, a realistic setup in experiments, and comparisons between the uniform and nonuniform flux.

[45] Only half of the period is shown. Because of the inversion symmetry and nonsymmorphic symmetry, there are, in general, 2 or 4 peaks in a period, $2\pi a_8/q$. As the approximation order increases, the decrease of the width of the wave function is accompanied by the increase of the period and the separation between peaks.

[46] H. Hiramoto and M. Kohmoto, Electronic spectral and wavefunction properties of one-dimensional quasiperiodic systems: A scaling approach, Int. J. Mod. Phys. B **06**, 281 (1992).

[47] R. B. Diener, G. A. Georgakis, J. Zhong, M. Raizen, and Q. Niu, Transition between extended and localized states in a one-dimensional incommensurate optical lattice, Phys. Rev. A **64**, 033416 (2001).